Modeling of Eigenvalues for MIMO Channel Capacity Based on Outdoor Measurements

Wonsop Kim, Hyuckjae Lee
School of Engineering
Information and Communications University
103-6, Munji-dong, Yuseong-gu, Daejon, 305-732, Korea
E-mail: {topsop, hjlee}@icu.ac.kr

Jae Joon Park, Myung-Don Kim, Hyun Kyu Chung
Mobile Telecommunication Research Laboratory
Electronics and Telecommunications Research Institute
161, Gajeong-dong, Yuseong-gu, Daejeon, 305-700, Korea
E-mail: {jjpark, mdkim, hkchung}@etri.re.kr

***Abstract*— This paper aims at modeling of eigenvalues for 2×N (i.e., 2 transmit and N receive antennas) channel capacity based on non line-of-sight (NLOS) wideband outdoor measurements. Our channel sounding system is the Band Exploration and Channel Sounding System (BECS) 2005, which works at a carrier frequency of 3.7 GHz with 100 MHz bandwidth. From the measured data, we investigate transmit antenna correlation coefficient (TxACC), receive antenna correlation coefficient (RxACC), channel capacity and eigenvalues of HH^* where H and (*) are channel frequency response matrix and conjugate transpose. Based on eigenvalue characteristics, we derive mean and variance of eigenvalue which are a function of the absolute value of TxACC, |TxACC|, the absolute value of RxACC, |RxACC|, and the number of Rx antennas, and then model eigenvalues for 2×N channel capacity. Monte Carlo simulations are used to generate eigenvalue realizations according to the model. The results are compared with the measure data and good agreements are found.**

Keywords-antenna correlation; capacity; CDF; channel sounder;

I. INTRODUCTION

Multiple Input Multiple Output (MIMO) antenna systems have recently gained considerable interest as they offer high data throughput and significant enhancement in link reliability over single antenna technology, without requiring extra power or bandwidth. Since performance of MIMO system depends on the behavior of MIMO channel, efficient system for MIMO communication requires accurate knowledge of channel characteristics. Channel sounders [1-2] should therefore provide the temporal and spatial characteristics of the MIMO channel with accuracy and resolution high enough to befit the design purpose. As a time division multiplexing (TDM) based wideband MIMO channel sounder, the BECS 2005 system [3] working at a carrier frequency of 3.7 GHz with 100 MHz bandwidth was developed in ETRI.

In many realistic environment, MIMO channels exhibit some degree of correlation among the multiple transmit (Tx) and receive (Rx) antennas due to poor scattering environment or closely spaced antennas. Consequently, the achievable capacity in real propagation environment may be lower than theoretical capacity. Since the channel capacity is determined by the MIMO channel conditions, this has given a motive for characterizing and modeling MIMO channels.

This work was supported by the IT R&D program of KCC/IITA, [2005-S-001-03, Development of Wireless Vector Channel Model for Next Generation Mobile Communication]

In this paper, we have presented the TxACC, RxACC, channel capacity and eigenvalues. Based on eigenvalue characteristics, we derive the mean and variance values of eigenvalues which are a function of |TxACC|, |RxACC| and the number of Rx antennas. Monte Carlo simulations have been used and good agreements have been found by comparing the results from the measured data and those simulated using the model.

The paper is organized as follows. Section II gives a brief description of the measurement campaign. Section III presents the analysis of measurement data. In Section IV, we provide the eigenvalue model for 2×N channel. Finally, conclusions are given in Section V.

II. MEASUREMENT CAMPAIGN

Fig. 1 shows the measurement site of Daechi-dong, an urban macrocell environment, in Seoul, Korea. The measurement site includes office and apartment buildings, heights of which are from 2 to 10 strories. The Tx system uses a uniform linear array (ULA) consisting of two antennas, which are collinear dipole arrays respectively. The Rx system uses ULA consisting of eight antennas, which are quarter wave monopoles respectively. The Tx antenna array is located on the rooftop of 10 stories building and marked on the center of the Fig. 1 with Tx. The Rx antenna array is mounted on the roof of a car. From the starting point of each route, Loc_1 and Loc_2, we drive along each route at a speed of around 30 km/h. Surrounding buildings completely block the direct path from

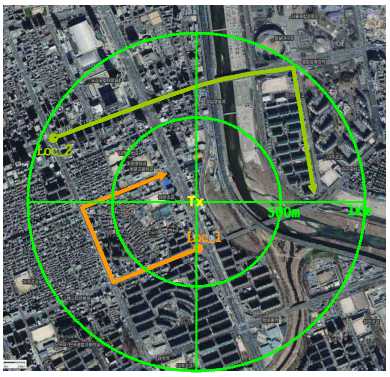

Figure 1. Measurement site: Tx array is located in the center of the map (yellow color); Loc_1 (orange color); Loc_2 (Green color)

TABLE I. MEASUREMENT ENVIRONMENT

Route	Tx Antenna Height [m]	Average Building Height [m] (Radius: from Tx to 1Km)
Loc_1 Loc_2	34	14.7

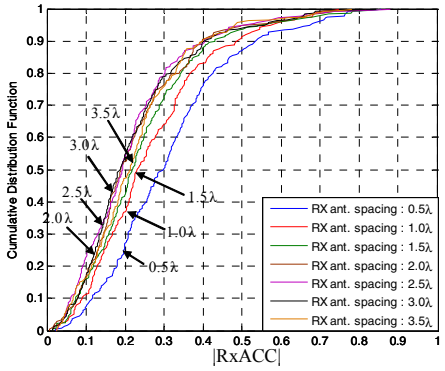

Figure 2. |RxACC| from measured channels

Tx to Rx and contribute to the diffractive and reflective paths. Thus, the routes are NLOS channel environments. Table I shows the measurement environment.

III. ANALYSIS OF MEASUREMENT DATA

A. MIMO Channel Matrix

A frequency-selective MIMO channel of M Tx and N Rx antennas can be represented by a channel matrix $\mathbf{H}(\tau) \in \mathbb{C}^{N\times M}$ defined as [4]

$$\mathbf{H}(\tau) = \sum_{\ell=1}^{L} \mathbf{A}^{(\ell)} \delta(\tau - \tau_\ell) \tag{1}$$

where L denotes the number of multipath components and the $\mathbf{A}^{(\ell)}$ at delay τ_ℓ is defined as

$$\mathbf{A}^{(\ell)} = \begin{bmatrix} \alpha_{11}^{\ell} & \alpha_{12}^{\ell} & \cdots & \alpha_{1M}^{\ell} \\ \alpha_{21}^{\ell} & \ddots & & \vdots \\ \vdots & & \ddots & \vdots \\ \alpha_{N1}^{\ell} & \cdots & \cdots & \alpha_{NM}^{\ell} \end{bmatrix} \in \mathbb{C}^{N\times M} \tag{2}$$

where α_{nm}^{ℓ} denotes the complex channel coefficient with m th Tx and n th Rx antennas.

B. Antenna Correlation

Let u, v be two complex random variables. The complex correlation coefficient is defined as

$$\rho_{complex} = \frac{\sum_{\ell=1}^{L} (u^{\ell} - \overline{u})(v^{\ell} - \overline{v})}{\sqrt{\sum_{\ell=1}^{L} \left|u^{\ell} - \overline{u}\right|^2 \sum_{\ell'=1}^{L} \left|v^{\ell'} - \overline{v}\right|^2}} \tag{3}$$

where $\overline{u}$ and $\overline{v}$ denote the sample means of the sets $\{u^{\ell}\}$ and $\{v^{\ell}\}$ with set size L, respectively. We calculate the correlation coefficient of two different Rx antennas from the same Tx antenna (RxACC) or of two different Tx antennas from the same Rx antenna (TxACC). Fig. 2 and Fig. 3 show the cumulative distribution functions (CDFs) of |RxACC| and |TxACC| calculated from measured channels. In Fig. 2, the Rx antenna spacing varies from 0.5λ to 3.5λ and Tx antenna spacing is fixed to 10λ. In Fig. 3, the Tx antenna spacing varies from 10λ to 30λ and Rx antenna spacing is fixed to 0.5λ. As expected, we can see that |RxACC| and |TxACC| decreases as Rx or Tx antenna spacing increases.

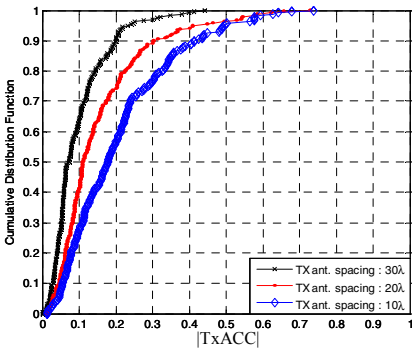

Figure 3. |TxACC| from measured channels

C. Capacity

From the channel frequency response matrices, the capacity of the wideband MIMO channel can be calculated by dividing the bandwidth of interest into Λ narrowband frequency bins. When the channel is unknown to the transmitter, the narrowband channel capacity C_{nb} is defined as [5]

$$C_{nb}(f) = \log_2 \det\left(\mathbf{I}_N + \frac{\psi}{M}\mathbf{H}(f)\mathbf{H}^{*}(f)\right) \quad [bits/s/Hz] \tag{4}$$

where $\mathbf{H}(f)$ is $N\times M$ channel frequency responses, $f = 1, 2, \cdots, \Lambda$ is narrowband frequency bin, $\mathbf{I}_N$ is the identity matrix, ψ denotes the average SNR. The narrowband channel capacity C_{nb} can be written as [6]

$$C_{nb}(f) = \sum_{i=1}^{r} \log_2\left(1 + \frac{\psi}{M}\lambda_i\right) \tag{5}$$

where r is the rank of the channel, λ_i is eigenvalue for $i = 1, \cdots, r$. The wideband MIMO channel capacity C_{wb} can be expressed as [5]

$$C_{wb} = \frac{1}{\Lambda}\sum_{f=1}^{\Lambda} C_{nb}(f). \tag{6}$$

To calculate the channel capacity, the measured channel matrices should be correctly normalized [5]. Since the rank of $\mathbf{H}(f)\mathbf{H}^{*}(f)$ for 2×N channel is no more than 2, we assume that there are two ordered eigenvalues, $\lambda_1 \le \lambda_2$. The probability density function (pdf) of gamma distributed random variables is given by [7]

$$f(x;k,\theta) = x^{k-1}\frac{e^{-x/\theta}}{\theta^k \Gamma(k)} \quad \text{for } x, k, \theta > 0 \tag{7}$$

where $\Gamma(\cdot)$ represents gamma function and x, k and θ are variable, shape and scale respectively. Fig. 4 shows the CDFs of gamma distributed random variables and λ_1 and λ_2 of

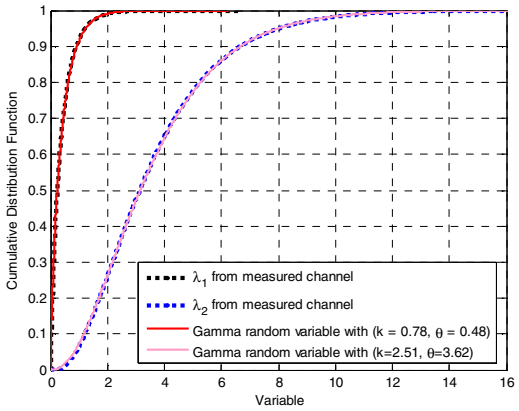

Figure 4. CDFs of gamma distributed random variables and eigenvalues for measured 2×2 channel

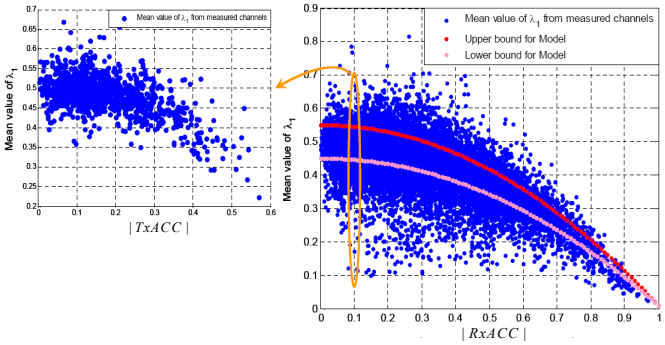

Figure 5. Mean value μ_1 of λ_1 with respect to |RxACC| in 2×2 channel (Right); μ_1 with respect to |TxACC| in 2×2 channel (Left)

measured 2×2 channel. It is observed that the distributions of λ_1 and λ_2 almost fit with gamma distribution.

IV. EIGENVALUE MODEL

A. Eigenvalue Characteristics

To model the eigenvalues, we use the eigenvalue characteristics of measured 2×2, 2×4, 2×6 and 2×8 channels. From Fig. 4, if we assume that eigenvalues are gamma distributed, then the mean and variance of eigenvalues satisfy [7]

$$E(\lambda) = k\theta,\ \mathrm{Var}(\lambda) = k\theta^2 \tag{8}$$

where $E(\bullet)$ and $\mathrm{Var}(\bullet)$ denote expectation and variance respectively. Since k and θ are key parameters to generate gamma distributed random variable, the θ and k are given by

$$\theta = \mathrm{Var}(\lambda)/E(\lambda),\ k = \{E(\lambda)\}^2/\mathrm{Var}(\lambda) \tag{9}$$

Fig. 5 shows the mean value μ_1 of λ_1 with respect to |RxACC| and |TxACC| respectively. In Fig. 5, the μ_1 of λ_1 with respect to |RxACC| ranges from 0 to 1 in 2×2 channel, when |TxACC| varies from 0 to 1. In Fig. 5, the μ_1 with respect to |TxACC| ranges from 0 to 1, when |RxACC| is fixed to 0.1. Fig. 6 shows the μ_1 with respect to |RxACC| in 2×2, 2×4, 2×6 and 2×8 channels. Fig. 7 shows the μ_2 with respect to μ_1 in 2×2, 2×4, 2×6

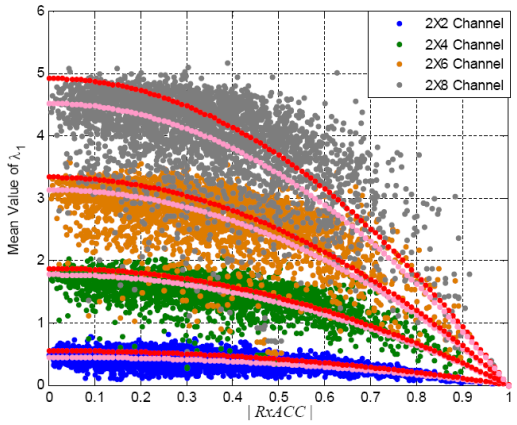

Figure 6. Mean value μ_1 of λ_1 with respect to |RxACC| in 2×2, 2×4, 2×6 and 2×8 channels

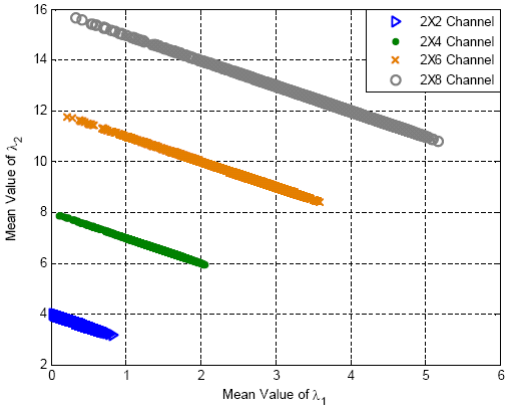

Figure 7. Mean value μ_2 of λ_2 with respect to mean value μ_1 of λ_1 in 2×2, 2×4, 2×6 and 2×8 channels

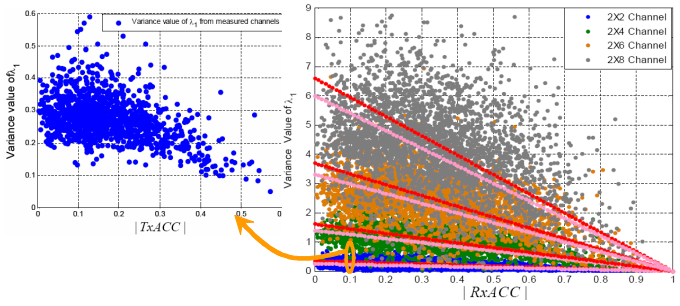

Figure 8. Variance value σ_1^2 of λ_1 with respect to |RxACC| in 2×2, 2×4, 2×6 and 2×8 channels (Right); σ_1^2 with respect to |TxACC| in 2×2 channel (Left)

and 2×8 channels. Fig. 8 shows the variance value σ_1^2 of λ_1 with respect to |RxACC| and |TxACC| respectively. Fig. 9 shows the σ_2^2 of λ_2 with respect to |RxACC| and |TxACC| respectively. In Fig. 6, 8 and 9, the red and purple lines are upper and lower bound, which mean that the range of |TxACC| $\in$ (0,1). From the measurement results, it is found that |RxACC|, |TxACC| and the number of Rx antennas have great influences on eigenvalue characteristics.

B. Eigenvalue Model

From the eigenvalue characteristics in Section IV A, we model

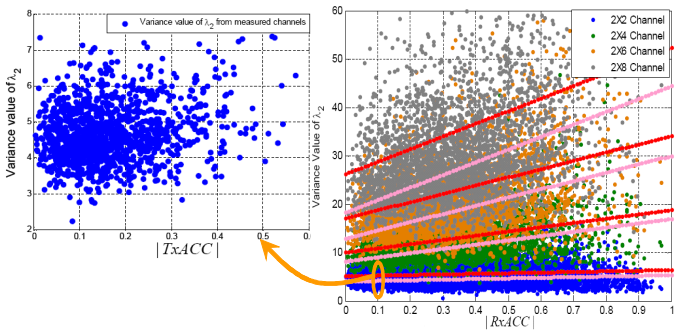

Figure 9. Variance value σ_2^2 of λ_2 with respect to |RxACC| in 2×2, 2×4, 2×6 and 2×8 channels (Right); σ_2^2 with respect to |TxACC| in 2×2 channel (Left)

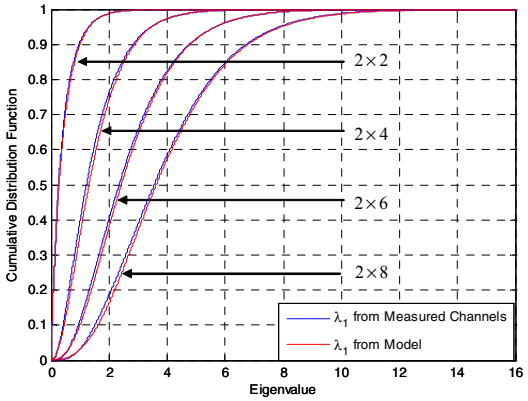

(a) CDFs of λ_1

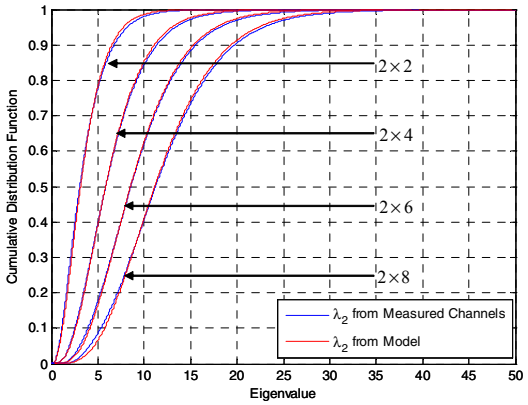

(b) CDFs of λ_2

Figure 10. Eigenvalue CDFs of measured channel and model in 2×2, 2×4, 2×6 and 2×8 channels

eigenvalues by deriving the mean and variance as a function of |RxACC|, |TxACC| and the number of Rx antennas. Firstly, we define the modeling conditions according to the following.

- μ_1 exponentially decreases as |RxACC| increase, when |TxACC| is fixed. (based on Fig. 5 and Fig. 6)
- μ_1 linearly decreases as |TxACC| increase, when |RxACC| is fixed. (based on Fig. 5 and Fig. 6)
- σ_1^2 linearly decreases as |RxACC| increase, when |TxACC| is fixed. (based on Fig. 8)
- σ_1^2 linearly decreases as |TxACC| increase, when |RxACC| is fixed. (based on Fig. 8)
- σ_2^2 linearly increases as |RxACC| increase, when |TxACC| is fixed. (based on Fig. 9)
- σ_2^2 linearly increases as |TxACC| increase, when |RxACC| is fixed. (based on Fig. 9)

The range of |TxACC| is defined as gab factor (GF). To find the optimized GF we define the wideband model error Φ as follows;

$$\Phi = \sum_{q=1}^{Q} \left| C_r^q - C_m^q \right| \tag{10}$$

where C_r^q and C_m^q are wideband real and model capacities for q th channel, Q is the total measured channels. By using Maximum Likelyhood (ML) method, The GFs of μ_1, σ_1^2 and σ_2^2 in 2×N channel are calculated by minimum mean square estimation (MMSE) fitting curves based on GF values which produce almost the least Φ and increase as the number of Rx antennas increase (2×2, 2×4, 2×6 and 2×8 cases). The GFs in 2×N channel are as follows;

$$\begin{aligned} GF_{\mu_1,2\times N} &= 0.0148\times(z)^2 - 0.0703\times z + 0.2094 \\ GF_{\sigma_1^2,2\times N} &= 0.0102\times(z)^2 + 0.4891\times z - 0.9094 \\ GF_{\sigma_2^2,2\times N} &= 0.0188\times(z)^2 + 1.0775\times z + 0.725 \end{aligned} \tag{11}$$

where z is the number of Rx antennas. From Fig. 6, 8 and 9, the slopes (SPs) of upper or lower bound in 2×N channel are calculated by MMSE fitting curves based on SP values of μ_1, σ_1^2 and σ_2^2 in 2×2, 2×4, 2×6 and 2×8 channels. The SPs in 2×N channel are as follows;

$$\begin{aligned} SP_{\mu_1,2\times N} &= 0.704\times z - 0.96 \\ SP_{\sigma_1^2,2\times N} &= 0.1\times(z)^2 - 0.1 \\ SP1_{\sigma_2^2,2\times N} &= 0.1\times(z)^2 + 3.14\times z - 5.4 \\ SP2_{\sigma_2^2,2\times N} &= 0.17\times(z)^2 + 1.24\times z + 1.46 \end{aligned} \tag{12}$$

From (11) and (12), the μ_1 for 2×N channel is derived by

$$\begin{aligned} GP_{\mu_1,2\times N} &= (0.5 - y)\times GF_{\mu_1,2\times N} \\ \mu_{1,2\times N} &= -(SP_{\mu_1,2\times N} + GP_{\mu_1,2\times N})\times x^2 + SP_{\mu_1,2\times N} + GP_{\mu_1,2\times N} \end{aligned} \tag{13}$$

where $x = |RxACC|$, $y = |TxACC|$ and $|RxACC|, |TxACC| \in (0,1)$. The σ_1^2 for 2×N channel is derived by

$$\begin{aligned} GP_{\sigma_1^2,2\times N} &= (0.5 - y)\times GF_{\sigma_1^2,2\times N} \\ \sigma_{1,2\times N}^2 &= -(SP_{\sigma_1^2,2\times N} + GP_{\sigma_1^2,2\times N})\times x + SP_{\sigma_1^2,2\times N} + GP_{\sigma_1^2,2\times N} \end{aligned} \tag{14}$$

The σ_2^2 for 2×N channel is derived by

$$\begin{aligned} GP_{\sigma_2^2,2\times N} &= (0.5 - y)\times GF_{\sigma_2^2,2\times N} \\ \sigma_{2,2\times N}^2 &= (SP1_{\sigma_2^2,2\times N})\times x + SP2_{\sigma_2^2,2\times N} + GP_{\sigma_2^2,2\times N} \end{aligned} \tag{15}$$

Since from Fig. 7, the μ_2 is perfectly inverse proportional to μ_1 and increases with constant ratio as the number of Rx antennas increase, the μ_2 is derived by

$$\mu_{2,2\times N} = -\mu_{1,2\times N} + 2\times z \tag{16}$$

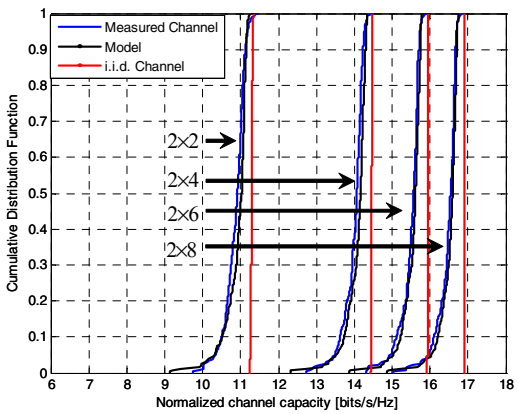

Figure 11. Capacity CDFs of measured channel, model and iid channel in 2×2, 2×4, 2×6 and 2×8 channels. The SNR is 20 dB.

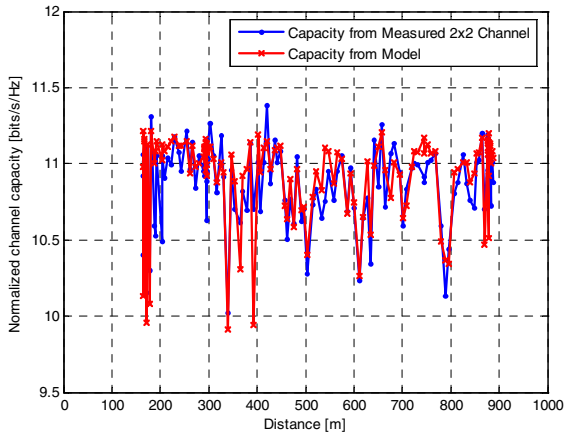

(a) 2x2 channel

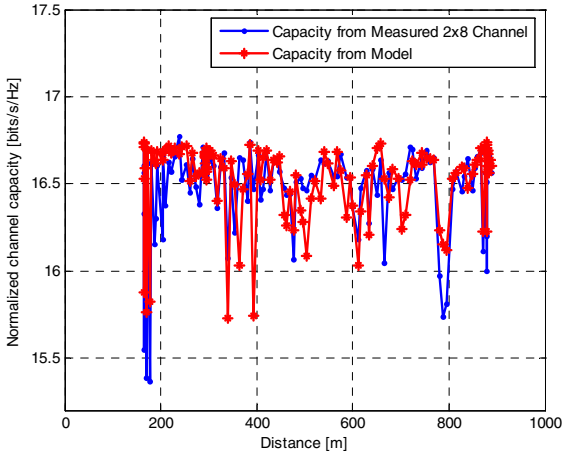

(b) 2x8 channel

Figure 12. Measured and model capacities with respect to distance in 2×2 and 2×8 channels

Given $\mu_{1,2\times N}, \mu_{2,2\times N}, \sigma^2_{1,2\times N}$ and $\sigma^2_{2,2\times N}$, the eigenvalues in 2×N channel can be modeled as

$$k_{i,2\times N} = \{\mu_{i,2\times N}\}^2 / \sigma^2_{i,2\times N},\ \theta_{i,2\times N} = \sigma^2_{i,2\times N} / \mu_{i,2\times N}$$
$$\lambda_{i,2\times N} \sim \Gamma(k_{i,2\times N}, \theta_{i,2\times N}), \qquad \text{for } i = 1,2 \tag{17}$$

where $\lambda_{i,2\times N}$ is gamma distributed with shape $k_{i,2\times N}$ and scale $\theta_{i,2\times N}$. Fig. 10 shows the eigenvalue CDFs of measured channel and model in 2×2, 2×4, 2×6 and 2×8 cases. We observe that the eigenvalue CDFs from model well fit to those from measured channels. Fig. 11 shows the capacity CDFs of measured channels and model with $\psi = 20\,\text{dB}$. As a reference, the capacity for the independent and identically distributed (i.i.d.) *CN* (0,1) channel is also included. There are good agreements between the model and measured capacities. Fig. 12 shows the examples of measured and model capacities with respect to distance in 2×2 and 2×8 channels. When |TxACC| and |RxACC| which are calculated form measured channels and vary with the measurement distance are used to model, it is observed that capacities from model well match with those from measured channels.

V. CONCLUSIONS

This paper has presented wideband MIMO measurements of NLOS outdoor channel. Our channel sounder BECS 2005 operate at a carrier frequency of 3.7 GHz with 100MHz bandwidth. By using the data, the MIMO channel statistical behaviors including antenna correlation coefficient, channel capacity and eigenvalues are presented. Eigenvalues are found to be Gamma distributed and the impact of TxACC, RxACC and the number of Rx antennas on eigenvalues has been demonstrated. Based on eigenvalue characteristics, we derive mean and variance of eigenvalues which are a function of |TxACC|, |RxACC| and the number of Rx antennas, and then model eigenvalues in 2×N channel. Monte Carlo simulations have been used and good agreements have been found by comparing the results from the measured data and those simulated using the model.

REFERENCES

[1] D. Chizhik, J. Ling. P. W. Wolniansky, R. A. Valenzuela, N. Costa, and K. Huber, "Multiple-Input-Multiple-Output Measurements and Modeling in Manhattan," *IEEE J. Select. Areas Commun.,* vol. 21, pp. 321-331, April 2003.

[2] M. D. Batariere, J. F. Kepler, T. P. Kauss, S. Mukthanvaram, J. W. Porter, and F. W. Vook, "An Experimental OFDM System for Broadband Mobile Communications, " in *Proc. IEEE VTC'01*, vol. 4, 2001, pp. 1947-1951.

[3] H. K. Chung, N. Vloeberghs, H. K. Kwon, S. J. Lee, and K. C. Lee, "MIMO channel sounder implementation and effects of sounder impairment on statistics of multipath delay spread," in *Proc. IEEE VTC'05*, vol. 1, 2005, pp. 349-353.

[4] D. P. Palomar, J. R. Fonollosa and M. A. Lagunas, "Capacity results of spatially correlated frequency-selective MIMO channels in UMTS," in *Proc. IEEE VTC'01,* vol. 2, 2001, pp. 7-11.

[5] Y. Yang, G. Xu, and H. Ling, "An Experimental Investigation of Wideband MIMO Channel Characteristics Based on Outdoor Non-LOS Measurements at 1.8 GHz," *IEEE Trans. Antennas Propag.,* vol. 54, pp. 3274-3284, Nov. 2006.

[6] J. P. Kermoal and L. Schumacher, "A Stochastic MIMO Radio Channel Model With Experimental Validation," *IEEE J. Select. Areas Commun.,* vol. 20, pp. 1211-1226, Aug. 2002.

[7] A. Leon-Garcia, *Probability and Random Processes for Electrical Engineering,* 2nd ed. Addison Wesley Publishing Company, 1994.